Mon. Not. R. Astron. Soc. **341,** 251–262 (2003)

Constraining dark energy from the abundance of weak gravitational lenses

Nevin N. Weinberg★ and Marc Kamionkowski
California Institute of Technology, Mail Code 130-33, Pasadena, CA 91125, USA

Accepted 2003 January 8. Received 2003 January 7; in original form 2002 October 8

ABSTRACT

We examine the prospect of using the observed abundance of weak gravitational lenses to constrain the equation-of-state parameter $w = p/\rho$ of dark energy. Dark energy modifies the distance–redshift relation, the amplitude of the matter power spectrum, and the rate of structure growth. As a result, it affects the efficiency with which dark-matter concentrations produce detectable weak-lensing signals. Here we solve the spherical-collapse model with dark energy, clarifying some ambiguities found in the literature. We also provide fitting formulae for the non-linear overdensity at virialization and the linear-theory overdensity at collapse. We then compute the variation in the predicted weak-lens abundance with w. We find that the predicted redshift distribution and number count of weak lenses are highly degenerate in w and the present matter density Ω_0. If we fix Ω_0 the number count of weak lenses for $w = -2/3$ is a factor of $\sim$2 smaller than for the Λ cold dark matter (CDM) model $w = -1$. However, if we allow Ω_0 to vary with w such that the amplitude of the matter power spectrum as measured by the *Cosmic Background Explorer* (*COBE*) matches that obtained from the X-ray cluster abundance, the decrease in the predicted lens abundance is less than 25 per cent for $-1 \leqslant w < -0.4$. We show that a more promising method for constraining dark energy – one that is largely unaffected by the Ω_0–w degeneracy as well as uncertainties in observational noise – is to compare the relative abundance of virialized X-ray lensing clusters with the abundance of non-virialized, X-ray underluminous, lensing haloes. For aperture sizes of $\sim$15 arcmin, the predicted ratio of the non-virialized to virialized lenses is greater than 40 per cent and varies by $\sim$20 per cent between $w = -1$ and -0.6. Overall, we find that, if all other weak-lensing parameters are fixed, a survey must cover at least $\sim$40 deg^2 in order for the weak-lens number count to differentiate a ΛCDM cosmology from a dark-energy model with $w = -0.9$ at the 3σ level. If, on the other hand, we take into account uncertainties in the lensing parameters, then the non-virialized lens fraction provides the most robust constraint on w, requiring $\sim$50 deg^2 of sky coverage in order to differentiate a ΛCDM model from a $w = -0.6$ model to 3σ.

Key words: gravitational lensing – galaxies: clusters: general – cosmology: miscellaneous.

1 INTRODUCTION

Observations of distant Type Ia supernovae (SNIa) indicate that the Universe is undergoing a phase of accelerated expansion (Perlmutter et al. 1999; Riess et al. 1998). Combined with the flat geometry favoured by cosmic microwave background (CMB) measurements (Miller et al. 1999; de Bernardis et al. 2002; Halverson et al. 2002; Sievers et al. 2002; Lee et al. 2001) and the evidence for a low matter density with $\Omega_0 \sim 0.3$ (Peacock 2001; Percival et al. 2001), this suggests that the bulk of the total energy density of the Universe is in the form of some exotic dark energy with a negative equation of state. One of the primary objectives of cosmology today is to uncover the origin and nature of this dark energy.

A possible candidate for dark energy is a cosmological constant Λ, with an equation of state $w = p/\rho$ (where p is the pressure and ρ is the energy density of dark energy) strictly equal to -1. Another possibility, and one that may find favour from a particle physics point of view, is a dynamical scalar field, termed quintessence, Q. Unlike the cosmological constant, the Q-component is both time-dependent and spatially inhomogeneous with an equation of state $w > -1$ that is likely to be redshift-dependent. The determination of the value of w and how it changes with time is the key to constraining the nature of dark energy.

★E-mail: nnw@tapir.caltech.edu

While the accelerating expansion implies only that $w < -1/3$, combinations of CMB data, SNIa data, and large-scale structure data suggest that w is most likely in the range $-1 \leqslant w < -0.6$ (Wang et al. 2000; Huterer & Turner 2001; Bean & Melchiorri 2002; Baccigalupi et al. 2002). Although the combination of these different data sets has provided some constraint on w, how w should vary with redshift is largely unknown. Particle physics offers several possible functional forms for the potential $V(Q)$ of the quintessence field and hence possible scenarios for the time history of w. None the less, determining the redshift evolution of w observationally is likely to be very challenging (Barger & Marfatia 2001; Maor, Brustein & Steinhardt 2001; Weller & Albrecht 2001).

However, it appears that strengthening the measured constraint on w and perhaps excluding the cosmological constant as the source of dark energy are attainable goals within the near future. Because the dark-energy dynamics influences both the evolution of the background cosmology and the growth of structure, it directly affects many observables. Its modification of the angular-diameter distance, the luminosity distance, and the amplitude of the matter power spectrum are the primary sources of dark-energy constraint in measurements of CMB anisotropies, SNIa, and local cluster abundances, respectively.

In this paper, we consider another possible means of constraining w: the measurement of weak gravitational-lens abundances. Weak lensing – the weak distortion of background-galaxy images due to the deep gravitational potential of an intervening overdensity – provides a powerful technique for mapping the distribution of matter in the Universe; see reviews by Bartelmann & Schneider (2001) and Mellier (1999). Here we study the impact of dark energy on the predicted redshift distribution and sky density of weak lenses. Dark energy affects the abundance of weak lenses not only by modifying the distance–redshift relation and the matter power spectrum but also by altering the rate of structure growth. In particular, the larger w is, the faster and earlier objects collapse. An interesting consequences of this is that if we separate weak lenses into the two observational classes – those that have collapsed and reached virial equilibrium and are therefore X-ray luminous and those that are non-virialized and hence X-ray underluminous (Weinberg & Kamionkowski 2002; hereafter WK02) – the abundance of one class evolves slightly differently from the other. Therefore, the relative fraction of these two types of lenses varies with w. This observable is especially promising as compared to measurements of absolute abundances because it is less sensitive to uncertainties in both the cosmological parameters and the noise in the lensing map.

This paper is organized as follows. In Section 2 we briefly summarize the weak-lensing signal-to-noise estimator and discuss how we determine the mass-dependent and redshift-dependent minimum overdensity required to produce a detectable weak-lensing signal. Section 3 is devoted to the spherical-collapse model in quintessence cosmologies. We provide fitting formulae for the non-linear overdensity at virialization and the linear-theory density at collapse, and we describe our approach to normalizing the matter power spectrum. In Section 4 we show the resulting effect dark energy has on the weak-lens abundances, and in Section 5 we present our conclusions.

Finally, we note that a similar analysis has recently been performed by Bartelmann, Perrotta & Baccigalupi (2002, hereafter BPB), although not for the case of non-virialized lenses. Although we agree with their general conclusion that the weak-lens abundance is a potentially sensitive probe of dark energy, our results differ from their results in important details. We discuss these differences in Section 4.2.

2 MINIMUM OVERDENSITY NEEDED TO PRODUCE DETECTABLE LENSING SIGNAL

In order to compute the abundance of weak gravitational lenses for dark-energy cosmologies we must first determine the necessary conditions for a halo of a given density profile and redshift to produce a detectable weak-lensing signal. Of course, the more overdense a halo is relative to the background density, the more it coherently distorts the nearby background galaxies and hence the stronger its lensing signal. The detectability of this signal is hampered, however, by noise in the weak-lensing map, primary of which is the intrinsic ellipticity distribution of the background galaxies. The goal is therefore to determine the minimum overdensity a halo must have such that it produces a sufficiently large signal relative to the noise so as to be detectable. A convenient method for computing this minimum overdensity is provided by the aperture-mass technique of Schneider (1996).

We consider a lens at redshift $z_{\rm d}$ of surface mass density $\Sigma(\vartheta)$ within an angular radius ϑ. For a source at redshift $z_{\rm s}$ the convergence κ is given by

$$\kappa(\vartheta) = \frac{\Sigma(\vartheta)}{\Sigma_{\rm crit}}, \qquad \Sigma_{\rm crit} = \frac{c^2}{4\pi G}\frac{D_{\rm s}}{D_{\rm d}D_{\rm ds}}, \tag{1}$$

where $D_{\rm d}$, $D_{\rm s}$ and $D_{\rm ds}$ are the angular-diameter distances between the lens and the observer, the source galaxy and the observer, and the lens and the source, respectively. Following Schneider (1996), we define a spatially-filtered mass inside a circular aperture of angular radius θ,

$$M_{\rm ap}(\theta) \equiv \int {\rm d}^2\boldsymbol{\vartheta}\kappa(\boldsymbol{\vartheta})U(|\boldsymbol{\vartheta}|), \tag{2}$$

where $U(\vartheta)$ is a continuous weight function that vanishes for $\vartheta > \theta$. If $U(\vartheta)$ is a compensated filter function,

$$\int_0^\theta {\rm d}\theta\boldsymbol{\vartheta}U(\boldsymbol{\vartheta}) = 0, \tag{3}$$

then $M_{\rm ap}$ can be expressed in terms of the tangential component of the observable shear, $\gamma_{\rm t}$,

$$M_{\rm ap}(\theta) = \int {\rm d}^2\vartheta\gamma_{\rm t}(\vartheta)Q(|\vartheta|), \tag{4}$$

where the function Q is related to U by

$$Q(\vartheta) = \frac{2}{\vartheta^2}\int_0^\vartheta {\rm d}\vartheta'\vartheta' U(\vartheta') - U(\vartheta). \tag{5}$$

In this paper we use the $l = 1$ radial filter function from the family given in Schneider et al. (1998),

$$U(\vartheta) = \frac{9}{\pi\theta^2}(1-x^2)\left(\frac{1}{3}-x^2\right),$$
$$Q(\vartheta) = \frac{6}{\pi\theta^2}x^2(1-x^2), \tag{6}$$

where $x = \vartheta/\theta$. Then, taking the expectation value over galaxy positions and taking into account the redshift distribution of source galaxies gives

$$M_{\rm ap}(\theta) = \langle Z\rangle \int {\rm d}^2\vartheta\langle\gamma_{\rm t}\rangle(\vartheta)Q(|\vartheta|), \tag{7}$$

where $\langle\gamma_{\rm t}\rangle$ (ϑ) is the mean tangential shear on a circle of angular radius ϑ. The function $\langle Z\rangle$, given by

$$\langle Z\rangle = \int {\rm d}z_{\rm s}p_z(z_{\rm s})Z(z_{\rm s};z_{\rm d}), \tag{8}$$

where $p_z(z_s)$ is the redshift distribution of source galaxies and (Seitz & Schneider 1997)

$$Z(z_s; z_d) \equiv \frac{\lim_{z_s\to\infty}\Sigma_{\rm crit}(z_d; z_s)}{\Sigma_{\rm crit}(z_d; z_s)} = \frac{\Sigma_{\rm crit_\infty}(z_d)}{\Sigma_{\rm crit}(z_d; z_s)} \quad (9)$$

allows a source with a known redshift distribution to be collapsed on to a single redshift z_s satisfying $Z(z_s) = \langle Z\rangle$ (Seitz & Schneider 1997; Bartelmann & Schneider 2001). The source–redshift distribution is taken to be

$$p_z(z_s) = \frac{\beta z_s^2}{\Gamma(3/\beta) z_0^3}\exp\left[-(z_s/z_0)^\beta\right], \quad (10)$$

with $\beta = 1.5$ and mean redshift $\langle z_s\rangle \approx 1.5\ z_0 = 1.2$ (cf. Smail et al. 1995; Brainerd, Blandford & Smail 1996; Cohen et al. 2000). Finally, assuming that the ellipticities of different images are uncorrelated it can be shown (cf. Kruse & Schneider 1999) that the dispersion $\sigma_M(\theta)$ of $M_{\rm ap}$ is

$$\sigma_M^2(\theta) = \frac{\pi\sigma_\epsilon^2}{n}\int_0^\theta {\rm d}\vartheta\,\vartheta\,Q^2(\vartheta), \quad (11)$$

where n is the number density of galaxy images and σ_ϵ is the dispersion in the galaxies' intrinsic ellipticity. In this paper we assume $n = 30$ arcmin^{-2} and $\sigma_\epsilon = 0.2$. The signal-to-noise ratio S within an aperture radius θ is then given by

$$S = \frac{M_{\rm ap}}{\sigma_M} = \frac{2\langle Z\rangle\sqrt{\pi n}}{\sigma_\epsilon}\frac{\int_0^\theta {\rm d}\vartheta\,\vartheta\,\langle\gamma_t\rangle(\vartheta)Q(\vartheta)}{\sqrt{\int_0^\theta {\rm d}\vartheta\,\vartheta\,Q^2(\vartheta)}}. \quad (12)$$

The tangential shear at ϑ, $\langle\gamma_t\rangle\,(\vartheta)$, depends on the amplitude and shape of the lensing halo's density profile. Bartelmann (1995) has shown that $\langle\gamma_t\rangle(\vartheta) = \bar\kappa(\vartheta) - \langle\kappa\rangle(\vartheta)$, where $\langle\kappa\rangle\,(\vartheta)$ is the dimensionless mean surface mass density on a circle of radius ϑ and $\bar\kappa(\vartheta)$ is the dimensionless mean surface mass density within a circle of radius ϑ. In this paper we describe the mass density of lensing haloes with the universal density profile introduced by Navarro, Frenk & White (NFW; 1996, 1997). Thus, for an NFW halo at a given redshift with a given mass and mean overdensity relative to the background ($\Delta \equiv \langle\rho_{\rm pert}\rangle/\rho_{\rm b}$), we can solve for the parameters of the profile (i.e. the scale radius and the scale density) and obtain an estimate of $\langle\gamma_t\rangle\,(\vartheta)$.

Because the details of how we solve for the NFW-profile parameters are given in the appendix of WK02 we do not repeat them here. Briefly describing the key points, we assume a collapse process analogous to that used by Dalcanton, Spergel & Summers (1997), in which the mass profile before collapse is a uniform sphere. We also assume that, as the overdensity collapses and approaches virialization, the mass distribution evolves into an NFW profile. Based on conservation of energy and mass we then obtain a halo concentration expressed in terms of the ratio between the turnaround radius and the scale radius. The benefit of such a procedure is that it enables us to solve for the NFW-profile parameters for both virialized and non-virialized systems, despite the fact that the concentration parameters quoted in the literature are for virialized systems only. We have compared the virialized halo concentration parameters inferred using this procedure with those obtained from numerical simulations and we have found that the two are roughly consistent with each other. For example, in our approach a 10^{14}-M$_\odot$ object at $z = 0$ has an NFW halo concentration c (defined as the ratio of the radius enclosing an overdensity of 200 to the scale radius) of 8.74 if $\Delta = 200$ and 6.53 if $\Delta = 100$, while numerical simulations typically yield values of $c \sim 7$ for virialized haloes.

Note too that, although N-body simulation fits to profiles have so far only been for virialized haloes, because most of the dark lenses are well past turnaround ($\Delta \gtrsim 100$) and because the Spherical Top Hat Collapse (STHC) model likely breaks down at some point before virialization, assuming an NFW profile for dark lenses is a fair approximation. Furthermore, as virialization occurs from inside out, the central regions of a dark lens, where most of the weak-lensing signal comes from, are likely to be near virialization and thus well described by the NFW form. Lastly, although we only consider the NFW profile in this paper, in WK02 we computed virialized and dark lens abundances assuming various types of other profiles including a uniform density sphere, the Hernquist profile (Hernquist 1990), and the isothermal sphere profile. Although the total number count of weak lenses does change for these different profiles, the normalized redshift distributions and the number count ratios of dark lenses to virialized lenses are largely unaffected. In this paper, we are chiefly concerned with the possibility of constraining the equation of state of dark energy via these differential, rather than cumulative, abundances. Assuming that the weak lenses have an NFW profile is therefore not crucial to the arguments or conclusions made herein.

With the density profile known we can determine, using equation (12), the expected value of S. The minimum mean overdensity, $\Delta_{\rm min}$, needed to produce a detectable lens is then given by that overdensity for which $S > S_{\rm min}$. In this paper we assume $S_{\rm min} = 5$ and $\theta = 5'$, unless stated otherwise.

3 SPHERICAL COLLAPSE IN DARK-ENERGY COSMOLOGIES

According to the spherical model of gravitational collapse, a density perturbation with a non-linear overdensity Δ corresponds to a particular position along the linear-theory evolutionary cycle. Thus the minimum non-linear overdensity $\Delta_{\rm min}$ described above corresponds to a minimum linear-theory overdensity $\delta_{\rm min}$; if an object of mass M at redshift z has a linear-theory overdensity $\delta > \delta_{\rm min} = \delta_{\rm min}(M, z)$, then it is sufficiently overdense to produce a detectable weak-lensing signal. By determining $\delta_{\rm min}$ from the computed $\Delta_{\rm min}$ we can apply the theory of Press & Schechter (1974) to calculate the number of haloes per unit mass and redshift with $\delta > \delta_{\rm min}$ and hence $S > S_{\rm min}$. We can then find the redshift distribution and sky density of weak lenses and how these observables vary with w. We show that for a broad range of dark-energy cosmologies a substantial fraction of detectable weak gravitational lenses have $\delta_{\rm min} < \delta_{\rm c} \approx 1.69$, where $\delta_{\rm c}$ is the critical density threshold for collapse. Those objects with $\delta < \delta_{\rm c}$ are commonly thought to be density perturbations that have not yet reached virialization and are therefore expected to have observational properties that are very different from typical virialized lensing clusters.

In this section, we present the approach used to map the minimum non-linear overdensity $\Delta_{\rm min}$ to a minimum linear-theory overdensity $\delta_{\rm min}$ for quintessence models (QCDM). We describe the dynamical equations of gravitational collapse in QCDM and give fitting formulae for the non-linear overdensity at virialization, $\Delta_{\rm vir}(z)$, and the critical density $\delta_{\rm c}$. We then discuss how we calculate the abundances of weak gravitational lenses, both those with $\delta < \delta_{\rm c}$ and those with $\delta > \delta_{\rm c}$. Below we assume a flat cosmology with a Hubble parameter $h = 0.65$, a spectral index $n_{\rm s} = 1$, a baryon density $\Omega_{\rm b}h^2 = 0.02$, and $\Omega_0 = 0.3$, unless stated otherwise.

3.1 Dynamics

In quintessence, the dark energy is a dynamical, time-dependent component, Q, with an equation of state parametrized by $w \equiv$

p_Q/ρ_Q, the pressure divided by the energy density. The evolution of the energy density with the cosmological scale factor goes as $\rho_Q \propto a^{-3(1+w)}$, so that for $w = -1$ the standard cosmological-constant model, ΛCDM, is recovered. Current observational evidence cannot yet rule out w in the range $-1 \leqslant w \lesssim -0.5$.

In order to relate a non-linear overdensity to a linear-theory overdensity in QCDM we must first solve for the evolution of the overdensity radius, R, with time. For a spherical overdensity patch with uniform matter density $\rho_{\rm pert} = 3M/4u\pi R^3$ the evolution is described by the momentum component of the Einstein equations (Wang & Steinhardt 1998; hereafter WS98):

$$\frac{\ddot{R}}{R} = -\frac{4\pi G}{3}[\rho_{\rm pert} + (1+3w)\rho_Q]. \tag{13}$$

As WS98 pointed out, for $w \neq -1$ the space curvature $k_{\rm pert}$ inside the overdensity patch is time-dependent. Physically, this is because the evolution of the energy density in the Q-component is evolving independently of the change in radius of the overdensity patch. As a result, we cannot assume that within the collapsing overdensity the rate of change of the internal energy in the Q-component, u_Q, equals the rate of work done by the Q-component. This is because $\mathrm{d}\rho_Q/\mathrm{d}t$ is non-zero unless the Q-component is the cosmological constant,

$$\frac{\mathrm{d}u_Q}{\mathrm{d}t} = \frac{d}{\mathrm{d}t}(\rho_Q V) \neq -p_Q\frac{\mathrm{d}V}{\mathrm{d}t}, \tag{14}$$

where $V \propto R^3$ is the volume of the overdensity patch. Therefore, equation (13) cannot be cast in the form of a first-order differential equation as is often done when going from an acceleration equation to a Friedman-like energy equation. Assuming a constant $k_{\rm pert}$, as was done in the first version preprint of Łokas & Hoffman (2001), yields significantly different solutions for the evolution of the radius, $R(t)$, and hence for $\Delta_{\rm vir}(z)$ and $\delta_{\rm c}$.

If we combine equation (13) with the Friedman equation for the background,

$$\left(\frac{\dot{a}}{a}\right)^2 = \frac{8\pi G}{3}(\rho_{\rm b} + \rho_Q), \tag{15}$$

and impose the boundary conditions $\mathrm{d}R/\mathrm{d}a|_{a=a_{\rm ta}} = 0$ and $R|_{a=0} = 0$, where $a_{\rm ta}$ is the scale factor at turnaround, then for a spherical density perturbation with a given Δ and redshift z, the unique temporal evolution of the overdensity, from linearity to non-linearity, can be solved (cf. Appendix A in WS98). We then have a one-to-one map from $\Delta(z)$ to $\delta(z)$, as shown in Fig. 1 for the cases $w = -1$, $-2/3$ and $-1/3$. The map has a mild w dependence, with a given δ corresponding to a slightly larger Δ as w increases. This is a consequence of the earlier formation of structure in QCDM models relative to ΛCDM models; overdensities collapse faster and are therefore more concentrated for $w > -1$. This point is well illustrated in Fig. 2 where we show the growth of a spherical perturbation for the same quintessence models. As expected, the larger w is, the earlier structures reach turnaround and collapse.

It can be shown that in the limit $\delta \to \delta_{\rm c}$ the spherical-collapse model predicts that the radius, R, of the overdensity goes to zero and hence $\Delta \to \infty$. Of course, well before reaching the singular solution an actual overdensity will virialize, thereby halting its collapse. To account for this fact we invoke a simple smoothing scheme in which the radius of the matter perturbation is constant with time upon reaching the virialized overdensity (see Fig. 2). We refer the reader to WK02 for details of the smoothing method.

As described in WS98, the value of $\Delta_{\rm vir}(z)$ for quintessence models, needed here in order to implement the smoothing scheme, can be obtained via the virial theorem, energy conservation, and solving equations (13) and (15) for the overdensity at turnaround. In Fig. 3 we show the resulting numerical solution to $\Delta_{\rm vir}(z)$. We find that an accurate fitting function to $\Delta_{\rm vir}(z)$ for $-1 \leqslant w \leqslant -0.3$, modelled after the approximation given in Kitayama & Suto (1996) for a ΛCDM cosmology, is

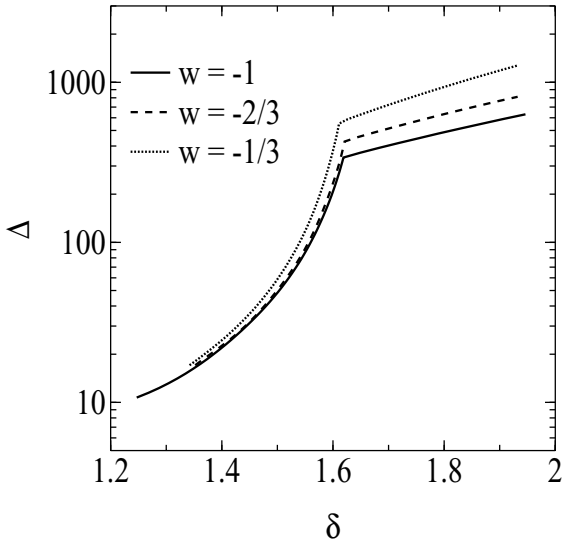

Figure 1. The non-linear overdensity as a function of the linear-theory overdensity for three constant-w models. The full solution of the spherical-collapse model predicts collapse to an infinite overdensity as $\delta \to \delta_{\rm c} \sim 1.69$. According to the smoothing scheme, however, once a mass concentration reaches the virialization overdensity $\Delta_{\rm vir}(z)$, its radius remains constant so that the overdensity increases in proportion to the decrease in the background density. Shown are the smoothing-scheme solutions for mass concentrations that reach the virialization overdensity at $z = 0$.

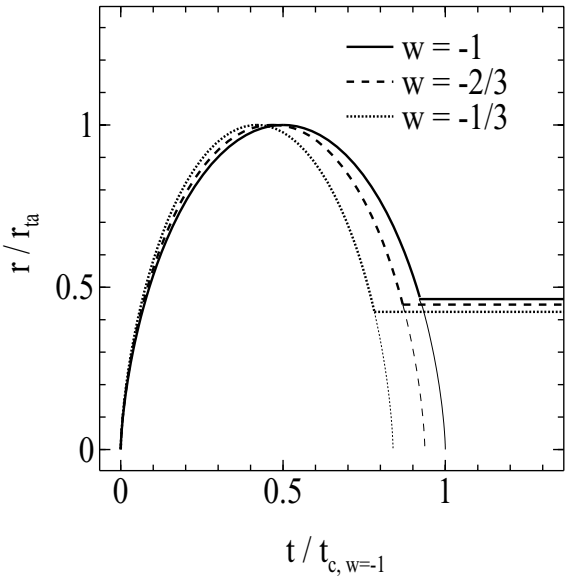

Figure 2. The radial evolution of a density perturbation that is collapsing today according to the spherical-collapse model. The ordinate gives the radius, r, in units of the turnaround radius, $r_{\rm ta}$, and the abscissa gives the time, t, in units of the overdensity collapse-time for the ΛCDM model. As w increases, perturbations reach turnaround and collapse earlier, although growth is suppressed earlier as well. The collapse to a singularity predicted by the solution of the spherical-collapse model is avoided by the smoothing scheme (thick curves) which yields a constant radius once the virialized overdensity is reached.

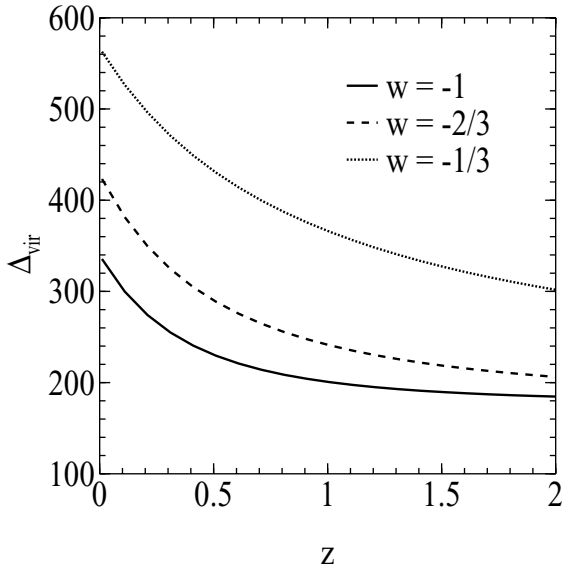

Figure 3. The non-linear overdensity at virialization as a function of redshift for three constant-w models. As w increases Δ_{vir} increases because overdensities collapse earlier, when the mean gas temperature was higher. For all models Δ_{vir} asymptotes to the Einstein–de Sitter value of 178 at high redshift.

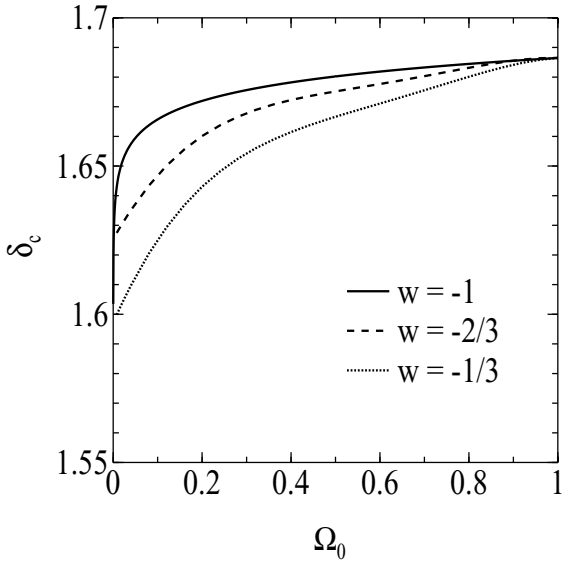

Figure 4. The linear-theory critical threshold for collapse, δ_c, at $z = 0$ as a function of Ω_0 for three constant-w models. δ_c does not vary significantly over a wide range in w or Ω_0.

$$\Delta_{vir}(z) = 18\pi^2[1 + a\Theta^b(z)], \tag{16}$$

where

$$a = 0.399 - 1.309(|w|^{0.426} - 1),$$
$$b = 0.941 - 0.205(|w|^{0.938} - 1), \tag{17}$$

and $\Theta(z) = 1/\Omega_m(z) - 1 = (1/\Omega_0 - 1)(1 + z)^{3w}$. As structures start to form earlier the larger w is, the mean gas temperature in collapsing objects is higher in larger-w models. As a result, a greater overdensity is required in order for such objects to become bound and virialized, explaining why Δ_{vir} rises with increasing w. Note, however, that for $\Delta(z) < \Delta_{vir}(z)$ the map from non-linear to linear overdensity has a weak dependence on not only w but on Ω_0 and redshift as well. The critical threshold for collapse today $\delta_c(z = 0) = \delta_c(z)\ D(0, \Omega_0, w)/D(z, \Omega_0, w)$, where $D(z, \Omega_0, w)$ is the linear growth factor (see WS98), also has a weak dependence on Ω_0 and w, as shown in Fig. 4. For $0.1 \leqslant \Omega_0 \leqslant 1$ and $-1 \leqslant w \leqslant -0.3$, we find that an accurate fitting function to $\delta_c(z)$, also modelled after the approximation given in Kitayama & Suto (1996) for a ΛCDM cosmology, is

$$\delta_c(z) = \tfrac{3(12\pi)^{2/3}}{20}[1 + \alpha \log_{10} \Omega_m(z)],$$
$$\alpha = 0.353w^4 + 1.044w^3 + 1.128w^2 + 0.555w + 0.131. \tag{18}$$

Incorrectly assuming that k_{pert} is constant, however, yields a $\delta_c(z = 0)$ with a much stronger dependence on these parameters, with inferred values for $\Omega_0 = 0.3$ of $\delta_c(z = 0) \sim 1.5$ and ~ 1.0 for $w = -2/3$ and $w = -1/3$, respectively (Łokas & Hoffman 2001).

3.2 Abundances

Because we are interested in computing the abundances of both virialized weak lenses and non-virialized weak lenses, we consider two ranges of overdensity in our lens-abundance calculations: (1) $\delta_{min} < \delta < \delta_c$, the non-virialized lenses; (2) $\delta > \delta_c \geqslant \delta_{min}$, the virialized lenses. As we have shown in WK02, the mass distribution of both the dark and virialized lenses peaks near $\sim 10^{14}$ $M_\odot$, although the virialized lenses' mass threshold of $\sim 10^{13}$ $M_\odot$ is several times *smaller* than that of the dark lenses (see WK02, figure 7). Although both types of lenses correspond to overdensities in a similar mass range, the virialized lenses are typically virialized clusters that form at rare (e.g. $> 3\sigma$) high-density peaks of a Gaussian primordial distribution, while the non-virialized lenses correspond to proto-clusters (e.g. 2σ–3σ peaks) – mass overdensities that have not yet undergone gravitational collapse and virialized, but which have begun to break away from the cosmological expansion. These proto-clusters should contain galaxies and perhaps a few groups that later merge to form the cluster (cf. White, van Waerbeke & Mackey 2002). The time-scale for collapse of cluster-mass objects is large, and the overdensities can be very large even before they have virialized. It should therefore not be too surprising that proto-clusters produce a weak-lensing signal that resembles that from virialized clusters.

Although the lensing signals may be similar, the two lens types are expected to have different observational features. In particular, as the X-ray luminosity is a very rapidly varying function of the virialized mass, the summed X-ray emission from a non-virialized lens should be much smaller than that from a fully virialized lensing cluster of the same mass. In referring to these proto-clusters as 'dark', we thus mean that they should be X-ray underluminous. Although the mass-to-light ratio of these clusters should be comparable to that for ordinary clusters, because (1) high-redshift clusters may be difficult to pick out in galaxy surveys and (2) proto-clusters will typically have a sky density a few times smaller than ordinary clusters, it would also not be surprising if these dark lenses had no readily apparent corresponding galaxy overdensity. Observational evidence of such dark lenses has been reported in detections by Erben et al. (2000), Umetsu & Futamase (2000), Miralles et al. (2002), Dahle et al. (2002) and Koopmans et al. (2000), the latter involving a detection through strong, rather than weak, lensing. A more detailed discussion of the features that may distinguish dark and virialized weak lenses is given in WK02.

As the weak-lensing signal reveals only the projected mass distribution, line-of-sight projection effects can lead to false halo detections. Using mock observations of numerical simulations White et al. (2002) have shown that the presence of large-scale structure results in projection effects that significantly limit the efficiency of a weak-lensing survey. Similarly, Hoekstra (2003) has shown that the combined effect of large-scale structure and the intrinsic ellipiticities of background galaxies can lead to 20–40 per cent errors in the determination of the mass of a lensing halo. Such effects will obviously hamper efforts to constrain cosmological parameters from cumulative number counts of weak lenses. However, it is important to note that, because the mass distributions of both dark lenses and virialized lenses are similar, false halo detections are not expected to affect the dark lenses any more than they do the virialized lenses. In fact, because the dark lenses have a larger mass threshold, a weak-lensing survey might be more efficient at detecting dark lenses than virialized lenses. Complementary observations in the optical and X-ray (and perhaps strong lensing and the Sunyaev–Zel'dovich effect) will clearly help to minimize the number of false detections. Although virialized lenses might benefit more from such follow-up observations, dark lenses will likely benefit as well, as they are expected to have a slight overdensity of galaxies as compared to the field and also perhaps emit a weak X-ray signal. Therefore, even though systematic uncertainties such as false halo detections might render the absolute number count of dark or virialized lenses impractical as a means of constraining cosmological parameters, the relative number count of dark to virialized lenses remains a viable option because both lens types are, for the most part, equally affected by such systematics. Of course, these conclusions are based on the simplifying assumptions inherent in the STHC model. It would therefore be very interesting to compare the analytical weak-lensing results obtained in this paper with numerical simulation predictions, in which non-virialized haloes are considered in addition to the oft-considered virialized haloes. This would provide an independent means of quantifying the completeness of future weak-lensing halo searches for both virialized and dark lenses. However, that comparison is beyond the scope of this paper.

Turning now to the details of the calculational method, in order to compute the abundances of virialized and dark lenses we need to know the probability that an object of a given mass at a given redshift is in one of the above-mentioned ranges in overdensity. If we assume Gaussian statistics for the initial linear-theory density field, then the probability that an object's overdensity is in the range $\delta_1 < \delta < \delta_2$ is

$$P(\delta_1 < \delta < \delta_2) = \mathrm{erf}\left(\frac{\nu_2}{\sqrt{2}}\right) - \mathrm{erf}\left(\frac{\nu_1}{\sqrt{2}}\right), \tag{19}$$

where 'erf' is the error function, $\nu = \delta/\sigma$, and $\sigma = \sigma(M, z)$ is the rms density fluctuation of an object of mass M at redshift z. From the Press–Schechter theory, we have that the comoving number density of virialized objects (those with $\delta > \delta_c$) of mass $M = 4\pi R^3 \rho_0/3$ in the interval d M that are at redshift z in a universe with comoving background density ρ_0 is

$$\frac{\mathrm{d}n}{\mathrm{d}M}(M, z) = \sqrt{\frac{2}{\pi}} \frac{\rho_0}{M^2} \frac{\delta_c(z)}{\sigma(M, z)} \left|\frac{\mathrm{d}\ln\sigma(M, z)}{\mathrm{d}\ln M}\right| \exp\left[-\frac{\delta_c(z)^2}{2\sigma^2(M, z)}\right]. \tag{20}$$

We can therefore compute the abundance of objects in the overdensity range $\delta_1 < \delta < \delta_2$ by convolving the above mass function of virialized objects with $P(\delta_1 < \delta < \delta_2)\,/\,P(\,\delta > \delta_c)$. Specifically, the fraction of objects that can lens relative to those that are virialized is, for dark lenses,

$$f_{\mathrm{dark}}(M, z) = \begin{cases} \frac{P(\delta_{\mathrm{min}} < \delta < \delta_c)}{P(\delta > \delta_c)}, & \delta_{\mathrm{min}} < \delta_c; \\ 0, & \text{otherwise}, \end{cases} \tag{21}$$

and for virialized lenses,

$$f_{\mathrm{vir}}(M, z) = \begin{cases} \frac{P(\delta > \delta_{\mathrm{min}})}{P(\delta > \delta_c)}, & \delta_{\mathrm{min}} > \delta_c; \\ 1, & \text{otherwise}. \end{cases} \tag{22}$$

As noted in WK02, the lower the mass of the object, the larger the minimum overdensity needed to produce a detectable weak-lensing signal. For low enough masses, the minimum overdensity becomes so large that both f_{dark} and f_{vir} approach zero, thereby imposing an effective weak-lensing mass threshold. It is worth noting that we have also considered the mass function suggested by Sheth & Tormen (1999), a variant of the Press–Schechter mass function that more accurately reproduces the mass functions found in numerical simulations. However, as the resulting lens abundances are essentially the same for both mass functions and because it is useful to compare our results with previous theoretical investigations of weak-lens abundances which often used the Press–Schechter mass function (e.g. Kruse & Schneider 1999), we only show results for the Press–Schechter mass function.

To summarize, given f and equation (20) we can compute the total comoving number density of weak lenses of a particular type. Multiplying by the comoving volume element $\mathrm{d}V_c/\mathrm{d}z\,\mathrm{d}\Omega\,(w)$ then gives the differential number count of lensing objects per steradian, per unit redshift interval:

$$\frac{\mathrm{d}N}{\mathrm{d}z\,\mathrm{d}\Omega} = \frac{\mathrm{d}V_c}{\mathrm{d}z\,\mathrm{d}\Omega} \int_0^\infty f(M) \frac{\mathrm{d}n}{\mathrm{d}M}(M)\,\mathrm{d}M. \tag{23}$$

By integrating over redshift we can then compute the number of dark and virialized lenses we expect to see per unit area of sky for a given QCDM model.

3.3 Normalizing the power spectrum

In equation (23) the volume term and the two terms within the integrand are all functions of w. While the predicted abundance of weak lenses will therefore vary with w, the degree to which it will vary depends on the shape and normalization of the power spectrum of density fluctuations. In particular, to compute the abundance of weak lenses we need to know $\sigma(M, z)$.

For the *shape* of the power spectrum we use the fitting formulae given in Ma et al. (1999) for QCDM models with the transfer function and shape parameter for ΛCDM models given by Bardeen et al. (1986) and Hu & Sugiyama (1996, equations D-28 and E-12), respectively. As the Q-component does not cluster on scales less than ∼100 Mpc (Caldwell, Dave & Steinhardt 1998), at the weak-lensing scales the shape of the spectrum does not differ significantly from the well-studied ΛCDM shape.

The *normalization* of the power spectrum, often expressed in terms of σ_8, the rms fluctuation today at a scale of 8 h^{-1} Mpc, is not as well constrained as its shape and will in general be a function of w. There are two different methods commonly used to obtain the normalization: to fix it by the observed X-ray cluster abundance or to fix it by the CMB large-scale anisotropies observed by the *Cosmic Background Explorer* (*COBE*) satellite. Both approaches have comparable uncertainties; the cluster abundance constraint on σ_8 has a 20 per cent uncertainty at the 2σ level (WS98) while the *COBE* constraint has a 7 per cent uncertainty at the 1σ level (Bunn

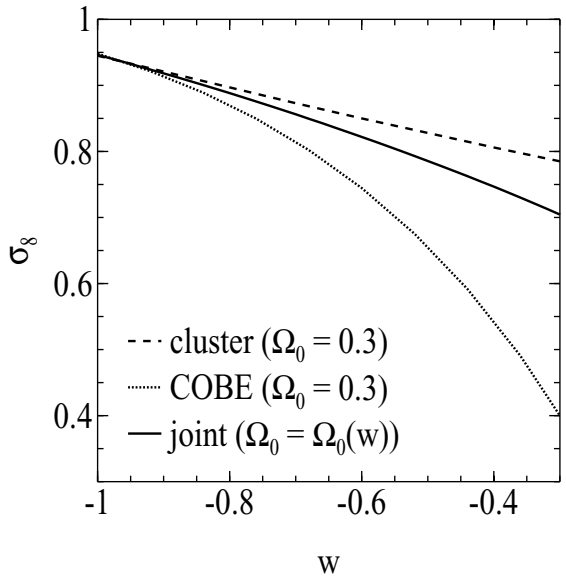

Figure 5. The dependence of σ_8 on w as obtained using three different approaches: fixing $\Omega_0 = 0.3$ and normalizing to the observed X-ray cluster abundance (dashed line); fixing $\Omega_0 = 0.3$ and normalizing to *COBE* (dotted line); and allowing Ω_0 to vary with w such that the cluster abundance constraint matches the *COBE* constraint (solid line).

& White 1997). To obtain an estimate of how σ_8 varies with w so that we may, in turn, determine how $\mathrm{d}N/\mathrm{d}z\ \mathrm{d}\Omega$ varies with w for dark and virialized lenses, we consider three possible approaches. The first two involve fixing the cosmological parameters (e.g. Ω_0, h, Ω_b, n_s) and using either the cluster-abundance constrained $\sigma_8(w)$ or the *COBE* constrained $\sigma_8(w)$. For the former we use the fit given in WS98 and for the latter the fit given by Ma et al. (1999); see Fig. 5. The third approach is to allow the cosmological parameters to be free parameters and then jointly match the cluster-abundance constraint with the *COBE* constraint so that each gives the same

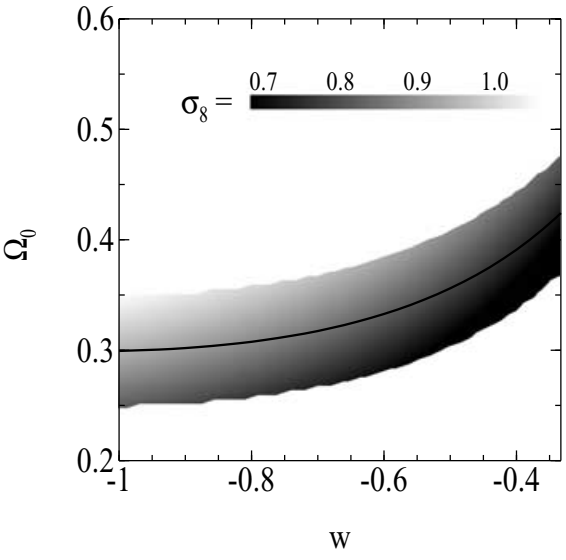

Figure 6. The region in the Ω_0–w plane where the X-ray cluster abundance constraint of σ_8, at 95 per cent confidence, overlaps the *COBE* constraint of σ_8. The grey-scale gives the corresponding σ_8 values and the solid line shows where the central values match.

$\sigma_8(w)$. As measurements of σ_8 are most degenerate with Ω_0, we let Ω_0 be the parameter that varies. In Fig. 6 we show the region in the Ω_0–w plane where the X-ray cluster-abundance constraint, at the 95 per cent confidence level, overlaps the *COBE* constraint. The solid curve shows where the central values match, with the resulting range in Ω_0 ($0.3 \lesssim \Omega_0 \lesssim 0.4$ for $-1 < w < -0.4$) within observational uncertainties (Wang et al. 2000). The corresponding $\sigma_8(w)$ curve is shown in Fig. 5. As we will show, the predicted weak-lens abundances and how they vary with w strongly depend on which $\sigma_8(w)$ normalization approach is chosen.

4 RESULTS

We are interested in determining whether the number count and redshift distribution of both dark and virialized weak lenses have the potential to constrain w. Another possibly useful observable for this purpose is the number count of dark lenses relative to virialized lenses. As dark lenses are at an earlier stage of their dynamical evolution as compared to virialized lenses, those cosmologies that favour a faster growth of structure (i.e. QCDM models with larger w) will, for a given σ_8, have fewer dark lenses and more virialized lenses. The ratio of the two is therefore expected to vary with w. A priori, this latter observable seems particularly promising. As discussed in WK02, the ratio of dark to virialized lenses is not very sensitive to observational noise in the weak-lensing maps because observational noise equally affects the detectability of both types of lenses. In contrast, uncertainties in observational noise will make it difficult to constrain w by simply comparing predicted weak-lens number counts with observed weak-lens number counts.

Before presenting how the above observables are modified by dark energy we first discuss how each of the factors that determine the observed abundance is affected by changes in w. Doing so provides both physical insight into the results and illustrates the calculational procedure discussed in the previous sections.

4.1 Preliminaries

As noted above, the predicted abundance of weak lenses will vary with w on account of three factors: the comoving volume element, the Press–Schechter comoving number density of virialized objects, and the value of $f_{\mathrm{dark/vir}}$ (equations 21 and 22). The degree to which each varies depends on the chosen $\sigma_8(w)$ normalization. As Fig. 7 shows, $\mathrm{d}V_\mathrm{c}/\mathrm{d}z\ \mathrm{d}\Omega$ decreases monotonically with increasing w for both fixed Ω_0 and $\Omega_0 = \Omega_0(w)$ as given by jointly normalizing σ_8 to *COBE* and the cluster abundance. However, because the joint normalization yields a larger Ω_0 with w and a less significant decline in σ_8 for $w > -1$ as compared to the *COBE* normalization with Ω_0 fixed, the former approach predicts a nearly constant virialized object number density with increasing w while the latter predicts a significant decrease in the number density.

A similar trend is seen in the functions f_{vir} and f_{dark}, as Fig. 8 demonstrates. Here we plot the fraction of objects that have not yet reached turnaround ($0 < \Delta < \Delta_{\mathrm{ta}}$) and the fraction of objects that are between turnaround and virialization ($\Delta_{\mathrm{ta}} < \Delta < \Delta_{\mathrm{vir}}$) relative to those objects that are virialized ($\Delta > \Delta_{\mathrm{vir}}$). The figure illustrates several key elements of structure formation according to the spherical-collapse model for dark-energy cosmologies. First, the fraction, χ, of objects in both of these lower-overdensity ranges increases with mass in accordance with the hierarchical growth of structure. The fraction also increases with redshift as objects are collapsing and evolving toward virialization. It is also interesting

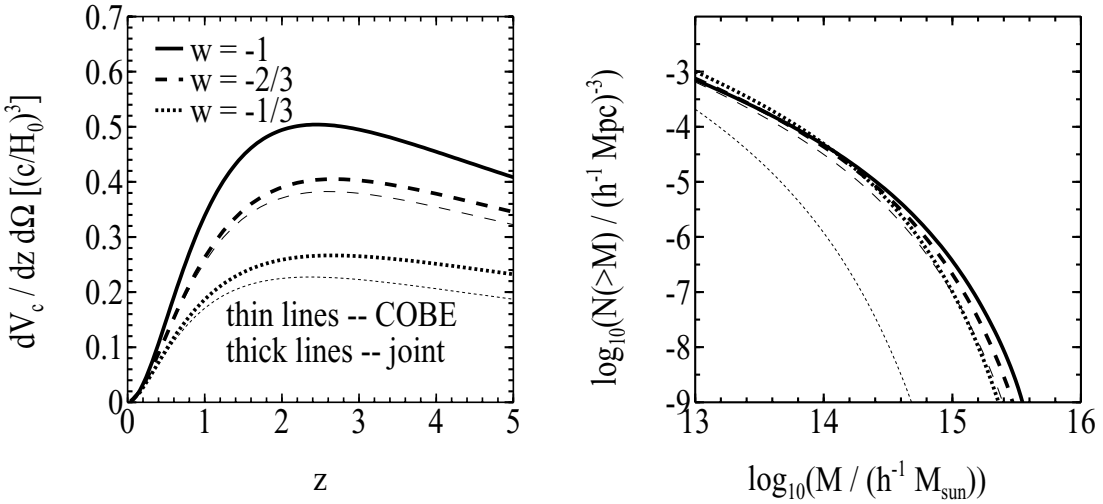

Figure 7. The comoving volume element as a function of redshift (left panel) and the comoving number density of virialized objects as a function of mass (right panel) for three constant-w models. Results are shown for both the *COBE* normalization of σ_8 with fixed $\Omega_0 = 0.3$ (thin lines) and the joint cluster abundance–*COBE* normalization of σ_8 with $\Omega_0 = \Omega_0(w)$ (thick lines).

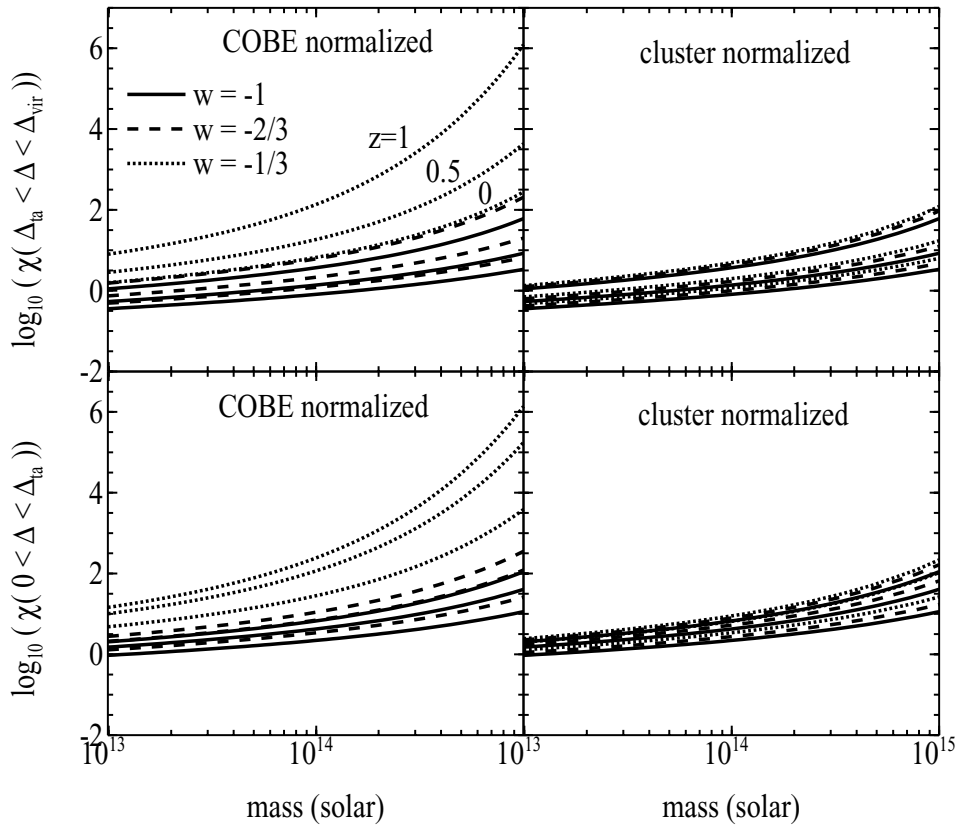

Figure 8. The fraction χ of objects with overdensities in the range $\Delta_{\rm ta} < \Delta < \Delta_{\rm vir}$ (upper panels) and $0 < \Delta < \Delta_{\rm ta}$ (lower panels) relative to those objects that are virialized, $\Delta > \Delta_{\rm vir}$, as a function of mass. The left panels correspond to the *COBE* normalization of σ_8 with $\Omega_0 = 0.3$, and the right panels correspond to the X-ray cluster abundance normalization of σ_8 with $\Omega_0 = 0.3$. For each constant-w model we show the fraction χ at $z = 0$ (bottom curve), $z = 1/2$ (middle curve) and $z = 1$ (top curve).

to note that objects with $\Delta_{\rm ta} < \Delta < \Delta_{\rm vir}$ evolve more rapidly as compared to objects with $0 < \Delta < \Delta_{\rm ta}$. This is demonstrated by the fact that at $z = 1$ the fraction of both types of objects is nearly the same, although by $z = 0$ there are more objects that have not reached turnaround. Furthermore, the larger w is, the greater the difference between the rates of evolution. These effects are a consequence of the suppression of structure growth in cosmologies with dark energy; namely, growth slows down earlier for larger w and those objects that are less overdense at a given redshift have greater difficulty overcoming the repulsive effects of dark energy and collapsing.

Finally, the plots show how strongly the fraction depends on the chosen σ_8 normalization, with a significant variation with w for the *COBE* normalization and a fairly small variation for the cluster-abundance normalization. This, in turn, means that the degree to which the functions $f_{\rm vir}$ and $f_{\rm dark}$ vary with w is highly dependent on the assumed normalization approach.

4.2 Weak-lens abundances

In Fig. 9 we show the predicted redshift distribution of virialized lenses and dark lenses for three constant w models. For the *COBE* normalized σ_8 with fixed Ω_0 the distributions show a fairly strong sensitivity to w. As w increases from -1 to $-1/3$ the peak of the distributions shifts towards lower redshift. Although we might expect the trend to be in the opposite direction given that structures form faster for larger w models, the effect is counteracted by the decrease in σ_8 with increasing w. That the decrease in σ_8 so overwhelms any tendency for structure to form faster for $w > -1$ is not surprising given the weak w dependence in the Δ–δ map (Fig. 1) and in the function $\delta_{\rm c}(z)$ (Fig. 4). Note, however, that the shift in the distributions with w becomes much less significant if a joint *COBE*–cluster abundance normalization is assumed. Finally, given that dark lenses are likely progenitors of virialized clusters, it is not surprising that both normalization approaches predict that the dark lenses have a larger mean redshift than the virialized lenses.

To determine how well the weak-lens redshift distributions can constrain w we generated mock redshift data and determined (using the Kolmogorov–Smirnov test) the probability of differentiating two different constant-w models as a function of the number of lenses detected. We found that to differentiate a ΛCDM model from both $w = -0.6$ and $w = -0.9$ models at the 3σ level required, on average, approximately 200 weak lenses and 2000 weak lenses, respectively. As we show below, this corresponds to a survey coverage of $\sim$15 and $\sim$150 deg^2. Note, however, that for sufficiently wide surveys systematic uncertainties such as mass-redshift selection effects and lens density profiles might dominate the errors.

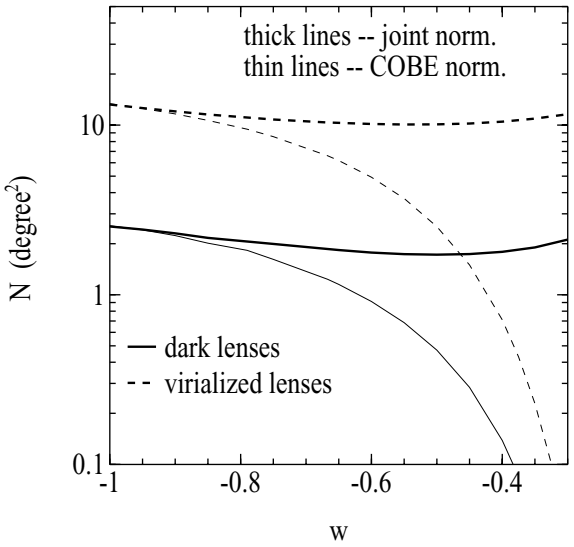

Figure 10. The total number of virialized lenses (dashed curves) and non-virialized lenses (solid curves) per deg^2 as a function of w. Thin lines correspond to the *COBE* normalized σ_8 with $\Omega_0 = 0.3$ and thick lines to the joint *COBE*–cluster abundance normalized σ_8 with $\Omega_0 = \Omega_0(w)$. While the number count drops by a factor of 2 between $w = -1$ and $w = -2/3$ for the *COBE*-only normalization, the drop is much less significant for the joint normalization.

By integrating over the redshift distribution we obtain the total number of virialized and dark lenses expected per deg^2 on the sky. As Fig. 10 shows, the *COBE* normalization with $\Omega_0 = 0.3$ shows a significant decline in the number count as w increases. By $w = -2/3$

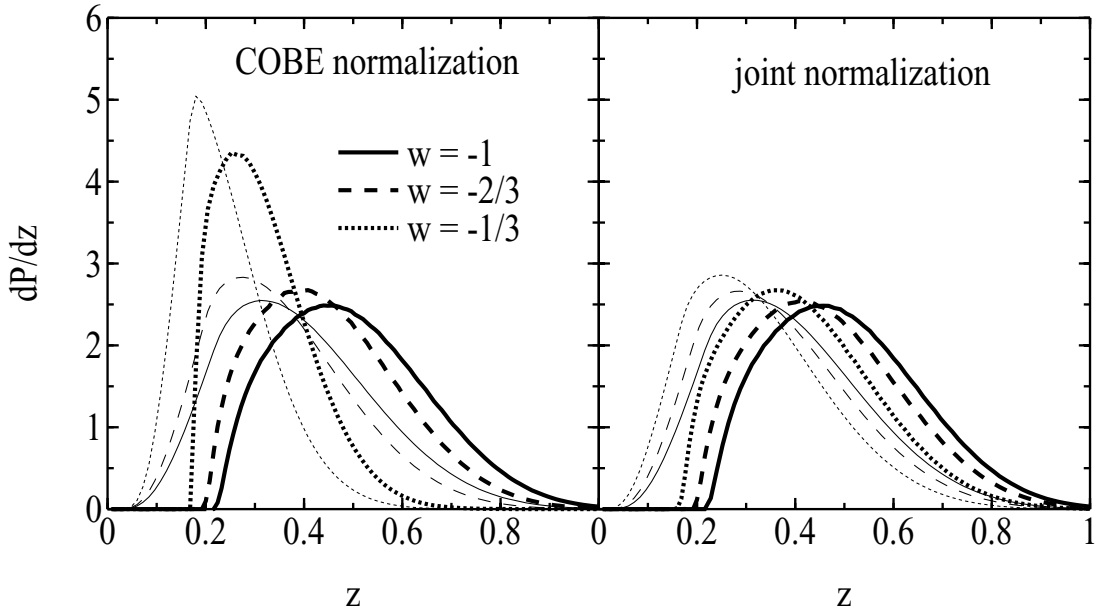

Figure 9. The normalized redshift distribution of virialized lenses (thin lines) and non-virialized lenses (thick lines) for three constant-w models. The left panel shows results obtained when σ_8 is normalized to *COBE* with $\Omega_0 = 0.3$, and the right panel when σ_8 is jointly normalized to *COBE* and the X-ray cluster abundance with $\Omega_0 = \Omega_0(w)$. The peaks of the redshift distributions shift toward lower redshift as w increases because σ_8 decreases with w. The shift in the peaks is less drastic, however, when the joint normalization is assumed.

the number count of both virialized and dark lenses has dropped by a factor of 2 from the ΛCDM value. The joint normalization, in which we allow Ω_0 to vary with w, predicts a much more mild dependence on w with the number count dropping by only ∼20 per cent from $w = -1$ to $-2/3$ for both lens types. Therefore, while the *COBE*-only normalization approach predicts that the sky coverage needed to distinguish the ΛCDM model from a $w = -0.6$ model to 3σ is only ∼2 deg^2, the joint approach requires ∼15 deg^2. Similarly, to distinguish the ΛCDM model from $w = -0.9$ requires ∼40 and ∼100 deg^2, respectively. The systematic uncertainties affecting absolute sky density measurements, such as noise in the lensing maps and uncertainties in the lens density profiles, are expected to add further complications. This suggests that it will be very difficult to constrain w using just the number count of either virialized or dark lenses without, at the very least, a tighter constraint on Ω_0.

We also note that our results do not agree with the results found by BPB. They found that from $w = -1$ to $w \approx -0.6$, the number of virialized weak lenses per deg^2 *increases* by nearly a factor of 2. The increase is roughly linear up to the maximum after which the number count declines steeply. In obtaining these results, however, they use the formulae for $\Delta_{\rm vir}$ and $\delta_{\rm c}$ given in Łokas & Hoffman (2001), who assume that the space curvature within a collapsing overdensity patch is time-independent. As we have shown in section 3.1, this assumption is invalid for $w \neq -1$ and leads to incorrect values for $\Delta_{\rm vir}$ and $\delta_{\rm c}$. To confirm that this is the source of our differences, we recomputed the number count of weak lenses as a function of w using the algorithm described in BPB (which differs from ours because we are interested in separating lenses into virialized and non-virialized types). When we assume the incorrect values of Łokas & Hoffman (2001) for $\Delta_{\rm vir}$ and $\delta_{\rm c}$ we recover the results found by BPB; however, when we assume the values for $\Delta_{\rm vir}$ and $\delta_{\rm c}$ predicted by solving the spherical-collapse equations of Section 3.1, we obtain results very similar to those described in the preceding paragraphs.

4.3 Fraction of lenses that are dark

As mentioned above, the number-count ratio of dark to virialized lenses is an observable that is much less sensitive to observational noise than is the redshift distribution and number count of weak lenses. Unfortunately, for aperture sizes θ (defined in Section 2) less than 10 arcmin in radius the ratio is fairly constant over a broad range in w, as we show in Fig. 11. The ratio varies more strongly if the aperture size is increased to 15 arcmin. In particular, for $\theta =$ 15 arcmin there is a ∼20 per cent difference between the ΛCDM model and $w = -0.6$, so that differentiating the two models to a 3σ significance requires the detection of ∼600 virialized lenses or equivalently a sky coverage of ∼50 deg^2. Although using the non-virialized lens fraction requires large survey coverage for modest constraints on w, its principal advantage (in addition to being relatively insensitive to observational noise) is that it is not very sensitive to the chosen method of normalization; for any aperture size, both the joint normalization and the *COBE* normalization with fixed Ω_0 yield similar dependences on w. Therefore, unlike the case for weak-lens sky-density or redshift distribution predictions, uncertainties in σ_8 and Ω_0 do not strongly affect the predicted ratio of dark to virialized lenses. Incidentally, although aperture sizes greater than ∼15 arcmin yield ratios with even stronger w dependences, noise contributions from large-scale structure become significant at such large angular distances from the lens centre (Hoekstra 2003). It is therefore not practical to make measurements at radii well beyond 15 arcmin.

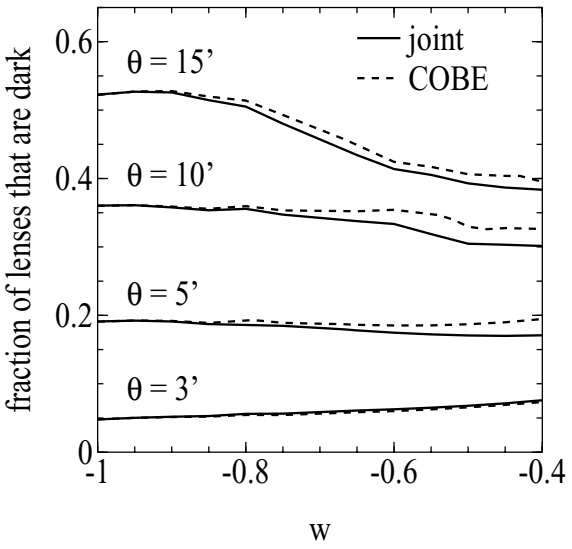

Figure 11. The fraction of lenses that are dark as a function of w for aperture sizes $\theta = 3$, *5*, 10 and 15 arcmin. Results are shown for both the *COBE* normalization with $\Omega_0 = 0.3$ (dashed lines) and the joint *COBE*–cluster abundance normalization with $\Omega_0 = \Omega_0(w)$ (solid lines). As θ increases, the fraction of lenses that are dark rises significantly.

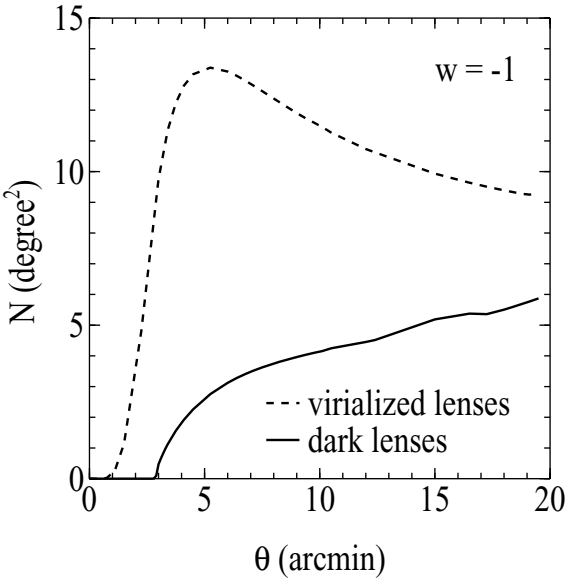

Figure 12. The total number of virialized lenses (dashed line) and non-virialized lenses (solid line) per deg^2 as a function of the aperture size θ for a ΛCDM cosmology. While the number count of virialized lenses peaks at $\theta = 5$ arcmin and declines thereafter, the number count of non-virialized lenses increases almost linearly for $\theta > 5$ arcmin.

As an aside, while the ratio of dark to virialized lenses does not have a particularly strong w dependence, it does have a strong θ dependence; only ∼5 per cent of lenses are dark when $\theta = 3$ arcmin but ∼50 per cent when $\theta = 15$ arcmin. In Fig. 12 we plot the number of virialized and dark lenses as a function of θ for the ΛCDM model. As θ increases from 3 to 15 arcmin the sky density of dark lenses increases from 0 to 5 per deg^2 while the sky density of virialized lenses peaks at $\theta = 5$ arcmin and gradually declines for larger aperture sizes. Fig. 13 explains this trend. For an overdensity of mass $M = 5 \times 10^{14}$ M$_\odot$ we plot, as a function of

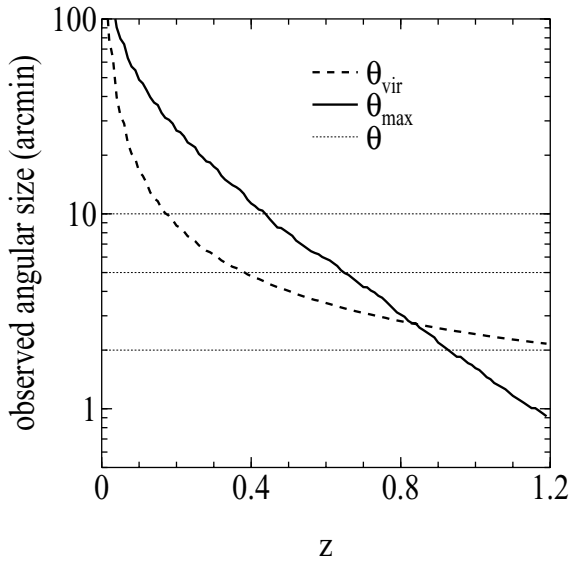

Figure 13. The observed angular size of $\theta_{\rm vir}$ (dashed line) and $\theta_{\rm max}$ (solid line) as a function of redshift for an overdensity of mass $M = 5 \times 10^{14}$ M$_\odot$ for a ΛCDM cosmology. If $\theta_{\rm max} > \theta_{\rm vir}$ an overdensity need not be virialized to produce a detectable lensing signal. However, the range in redshift over which a non-virialized lens can be detected is limited by the aperture size θ (e.g. thin dotted lines), which defines the maximum observable angular scale. For $\theta \lesssim 3$ arcmin, virtually no dark lenses can be detected.

redshift, $\theta_{\rm vir}$, the projected angular size of the virialization radius, and $\theta_{\rm max}$, the projected angular size of the maximum radius that produces a detectable lens [i.e. $\theta_{\rm max} = R_{\rm max}(z)/D_{\rm d}(z)$ where $R^3_{\rm max} = 3M/4\pi\ \Delta_{\rm min}(z)$]. For $\theta_{\rm max} > \theta_{\rm vir}$ an overdensity can be non-virialized and still produce a detectable lensing signal (i.e. a dark lens). However, as θ defines the maximum observable angular scale, for sufficiently small θ there is no range in redshift such that $\theta > \theta_{\rm max} > \theta_{\rm vir}$, in which case non-virialized overdensities cannot produce a detectable lens. In general, we find that the minimum aperture size needed to detect dark lenses is $\sim$3 arcmin. For larger θ, the area below $\theta_{\rm max}$ and above $\theta_{\rm vir}$ has a substantial relative increase while the area below $\theta_{\rm vir}$ has just a mild relative increase. After taking into account the fact that the aperture mass $M_{\rm ap}(\theta)$ decreases with increased θ, this translates to an increase in the sky density of dark lenses and a decrease in the sky density of virialized lenses for $\theta >$ 5 arcmin. The fraction of lenses that are dark therefore increases with aperture size.

5 DISCUSSION AND CONCLUSIONS

We have examined the possibility of using the measured abundance of weak gravitational lenses to constrain a principal property of dark energy, its equation-of-state parameter w. Because dark energy modifies both the background cosmology of the Universe and the growth of structure, it will necessarily have an effect on the efficiency of weak lensing. The goal of this paper was to determine the nature and strength of the effect.

The change in the background cosmology with w influences the predicted weak-lens abundance in essentially three ways. First, the size of comoving volume elements shrinks with increasing w. Secondly, the distance–redshift relation is modified, thereby shifting the location of the lensing-kernel maximum (i.e. where the combination of angular diameter distances $D_{\rm ds}D_{\rm d}/D_{\rm s}$ peaks). Thirdly, as the evolution of the background matter density is modified by dark energy, the density of a given halo relative to the background density changes with w. This, in turn, affects the strength of a halo's lensing signal; the larger the overdensity, the stronger the signal. While the volume term is explicitly factored into the expression for the weak-lens sky density (equation 22), the latter two effects are incorporated into the signal-to-noise estimator for which we use the aperture-mass technique introduced by Schneider (1996).

The change in the growth of structure with w is more subtle. The dark energy modifies both the rate of structure growth and the amplitude of the matter power spectrum. To determine the former we solved the spherical-collapse model with dark energy included. Although growth occurs more rapidly as w increases, the overall effect on the Δ–δ map, needed to relate the minimum overdensity required to produce a detectable lens, $\Delta_{\rm min}$, to a corresponding linear-theory overdensity $\delta_{\rm min}$, is fairly small. Similarly, the linear-theory overdensity at collapse $\delta_{\rm c}$ does not vary much with w. The effect on $\Delta_{\rm vir}$ is more significant, however. As w increases, structures require substantially greater overdensities in order to reach virial equilibrium because they collapse sooner, when the Universe was younger and hotter.

To determine how the power-spectrum amplitude, σ_8, varies with w we considered three possible approaches. One was to normalize to the X-ray cluster abundance, as was done in WS98. Another was to normalize to the *COBE* measurements of CMB anisotropies on large angular scales. These two approaches predict similar values of σ_8 for the ΛCDM model. However, if all cosmological parameters are held fixed as w varies, the values of σ_8 are no longer in accordance. This is because the cluster abundance approach accounts for the earlier-forming, and hence hotter, galaxy clusters in models with $w > -1$. The *COBE* normalization, on the other hand, accounts for the increase in the integrated Sachs–Wolfe (ISW) effect as w increases (cf. BPB). Given these differing influences, the two approaches are not expected to yield the same σ_8 when all the cosmological parameters are held fixed to those of the ΛCDM model while w is varied. This suggests a third approach to normalizing the power spectrum; namely, let the parameters vary with w such that the cluster abundance normalization matches the *COBE* normalization. In practice we accomplished this by letting just Ω_0 vary with w, as it is the parameter most degenerate with σ_8. The resulting range in Ω_0 for $-1 < w \lesssim -0.4$ was found to be $0.3 < \Omega_0 < 0.4$ and hence within observational uncertainties. Although all three normalization approaches predict that σ_8 decreases with w, the difference in the magnitude of the decrease between the approaches is significant. As a result, each predicts substantially different variations in the weak-lens abundance with w.

Having determined all the dark-energy effects, we computed the redshift distribution and sky density of weak lenses as a function of w. As in WK02, we distinguished between two classes of lenses: those that have collapsed and virialized and those that have not. This distinction is based on the expectation that the virialized lenses, being in a relaxed state, are X-ray and/or optically luminous. The non-virialized lenses, being at an earlier stage in the overdensity evolutionary cycle, are expected to be X-ray underluminous because the observed X-ray luminosity function has a steep dependence on the total virialized mass within a halo. Furthermore, although the typical mass of both lens types is $\sim$few $\times\ 10^{14}$ M$_\odot$, the sky density of galaxies within the non-virialized lenses is expected to be smaller than in the virialized lenses because they have not yet collapsed and hence have larger radii (see WK02 for more details).

We have found that the variation in the redshift distribution and the sky density of both lens types with w depends strongly on the power-spectrum-normalization approach. If Ω_0 is fixed and σ_8 is

normalized to the *COBE* measurements, there is a significant variation in the abundances with w. In particular, the sky density of both virialized lenses and non-virialized lenses drops by a factor of 2 from $w = -1$ to $w = -2/3$. This decline, a result of the significant decrease in σ_8 with w, occurs despite the faster formation of structure for $w > -1$. If, on the other hand, Ω_0 is allowed to vary with w such that the *COBE* normalization matches the cluster-abundance normalization, the redshift distributions and sky density change very little with w; between $w = -1$ and $w = -2/3$ the sky density of both lens types varies by just $\sim$20 per cent. This insubstantial variation is the result of an increase in Ω_0 with w and a less significant drop in σ_8 with w as compared to the *COBE* normalization with Ω_0 fixed. Obtaining a strong constraint on w from the sky density or redshift distribution of weak lenses therefore appears to be contingent on improved measurements of Ω_0 from independent observations.

Perhaps more promising is the possibility of utilizing the observed ratio of dark lenses to virialized lenses. Unlike measurements of the absolute sky density of weak lenses, the ratio is not very sensitive to the amount of observational noise in the weak-lensing maps as the abundances of both dark lenses and virialized lenses are equally affected by noise. Similarly, the ratio does not vary significantly over a wide range in cosmological parameters so that uncertainties due to the $\Omega_0 - w$ degeneracy are minimized. We found that for aperture sizes of $\sim$15 arcmin the ratio varies by about 20 per cent, dropping from 0.5 to 0.4, between the ΛCDM model and $w = -0.6$. We have also shown that the ratio of dark to virialized lenses increases with aperture size, in effect because larger apertures enable the detection of the more extended radii of the non-virialized lenses.

Weak lensing has already been shown to be a powerful probe of the matter distribution in the Universe (see, for example, Bartelmann & Schneider 2001). It also has the potential to help constrain the amount and nature of dark energy. Huterer (2002) has shown that, given reasonable prior information on other cosmological parameters, the weak-lensing convergence power spectrum can impose constraints on dark energy comparable to those of upcoming SNIa and number-count surveys of galaxies and galaxy clusters. Constraining dark energy from absolute measurements of weak-lens abundances will likely prove difficult, however. The variation in the weak-lens sky density with w is sufficiently small that modest uncertainties in Ω_0 (and observational noise) can mask the effect of dark energy. More auspicious is the possibility of utilizing the relative abundance of dark lenses to virialized lenses to constrain w. Future weak-lensing projects such as the Visible and Infrared Survey Telescope for Astronomy (VISTA), the Supernova/Acceleration Probe (SNAP) mission, and the Large-aperture Synoptic Survey Telescope (LSST) – see Tyson et al. (2002) for a discussion of its great promise as a probe of dark energy – are expected to provide the wide-field surveys needed for this technique to be viable.

ACKNOWLEDGMENTS

We thank R. Caldwell for helpful suggestions and an anonymous referee for useful comments that have improved the presentation of this paper. NNW acknowledges the support of an NSF Graduate Fellowship. This work was supported by NSF AST-0096023, NASA NAG5-9821, and DoE DE-FG03-92-ER40701.

REFERENCES

Baccigalupi C., Balbi A., Matarrese S., Perrotta F., Vittorio N., 2002, Phys. Rev. D, 65, 063520
Bardeen J. M., Bond J. R., Kaiser N., Szalay A. S., 1986, ApJ, 304, 15
Barger V., Marfatia D., 2001, Phys. Lett. B, 498, 67
Bartelmann M., 1995, A&A, 303, 643
Bartelmann M., Schneider P., 2001, Phys. Rep., 340, 291
Bartelmann M., Perrotta F., Baccigalupi C., 2002, A&A, 396, 21 (BPB)
Bean R., Melchiorri A., 2002, Phys. Rev. D, 65, 041302
Brainerd T. G., Blandford R. D., Smail I., 1996, ApJ, 466, 623
Bunn E. F., White M., 1997, ApJ, 480, 6
Caldwell R. R., Dave R., Steinhardt P. J., 1998, Phys. Rev. Lett., 80, 1582
Cohen J. G., Hogg D. W., Blandford R. D., Cowie, L. L., Hu, E., Songaila, A., Shopbell, P., Richberg, K., 2000, ApJ, 538, 29
Dahle H., Pedersen K., Lilje P. B., Maddox S. J., Kaiser N., 2002, ApJ, submitted (astro-ph/0208050)
Dalcanton J. J., Spergel D. N., Summers F. J., 1997, ApJ, 482, 659
de Bernardis P. et al., 2002, ApJ, 564, 559
Erben T., van Waerbeke L., Mellier Y., Schneider P., Cuillandre J.-C., Castander F. J., Dantel-Fort M., 2000, A&A, 355, 23
Halverson N. W. et al., 2002, ApJ, 568, 38
Hernquist L., 1990, ApJ, 356, 359
Hoekstra H., 2003, MNRAS, 339, 1155
Hu W., Sugiyama N., 1996, ApJ, 471, 542
Huterer D., 2002, Phys. Rev. D., 65, 063001
Huterer D., Turner M. S., 2001, Phys. Rev. D, 64, 123527
Kitayama T., Suto Y., 1996, ApJ, 469, 480
Koopmans L. V. E. et al., (CLASS collaboration), 2000, A&A, 361, 815
Kruse G., Schneider P., 1999, MNRAS, 302, 821
Lee A. T. et al., 2001, ApJ, 561, L1
Łokas E. L., Hoffman Y., 2001, preprint (astro-ph/0108283)
Ma C.-P., Caldwell R. R., Bode P., Wang L., 1999, ApJ, 521, L1
Maor I., Brustein R., Steinhardt P. J., 2001, Phys. Rev. Lett., 86, 6
Mellier Y., 1999, ARA&A, 37, 127
Miller A. D. et al., 1999, ApJ, 524, L1
Miralles J. M. et al., 2002, 388, 68
Navarro J. F., Frenk C. S., White S. D. M., 1996, ApJ, 462, 563
Navarro J. F., Frenk C. S., White S. D. M., 1997, ApJ, 490, 493
Peacock J. A., Nat, 2001, 410, 169
Percival W. J. et al., 2001, MNRAS, 327, 1297
Perlmutter S. et al., 1999, ApJ, 517, 565
Press W. H., Schechter P., 1974, ApJ, 187, 425
Riess A. G. et al., 1998, AJ, 116, 1009
Schneider P., 1996, MNRAS, 283, 837
Schneider P., van Waerbeke L., Jain B., Kruse G., 1998, MNRAS, 296, 873
Seitz C., Schneider P., 1997, A&A, 318, 687
Sheth R. K., Tormen G., 1999, MNRAS, 308, 119
Sievers J. L. et al., 2002, ApJ, submitted (astro-ph/0205387)
Smail I., Hogg D. W., Yan L., Cohen J. G., 1995, ApJ, 449, L105
Tyson J. A., Wittman D. M., Hennawi J. F., Spergel D. N., 2002, in Cline D., ed., Proc. 5th Int. UCLA Symp. on Sources and Detection of Dark Matter
Umetsu K., Futamase T., 2000, ApJ, 539, 5
Wang L., Caldwell R. R., Ostriker J. P., Steinhardt P. J., 2000, ApJ, 530, 17
Wang L., Steinhardt P. J., 1998, ApJ, 508, 483 (WS98)
Weinberg N. N., Kamionkowski M., 2002, MNRAS, 337, 1269 (WK02)
Weller J., Albrecht A., 2001, Phys. Rev. Lett., 82, 896
White M., van Waerbeke L., Mackey J., 2002, ApJ, 575, 640

This paper has been typeset from a TEX/LATEX file prepared by the author.